Applications of Interferometric Signal Processing to Phase-Noise Reduction in Microwave Oscillators

Eugene N. Ivanov, Michael E. Tobar, *Associate Member, IEEE,* and Richard A. Woode

***Abstract*—To enhance the sensitivity of oscillator phase-noise measurements, an interferometric frequency-discriminator system may be implemented. Such systems consists of a microwave interferometer, incorporating a high-Q resonator and a phase-sensitive microwave readout. Suppressing the carrier at the output of the interferometer enables the microwave readout to operate in the small-signal regime with an effective noise temperature close to its physical temperature. When used as a sensor of a frequency-control system to lock the oscillator to a selected resonant mode of a high-Q resonator, the interferometric frequency discriminator has enabled more than two orders of magnitude improvement in oscillator phase-noise performance as compared with the state-of-the-art. Thus, the phase noise of an X-band oscillator was reduced to -150 dBc/Hz at 1-kHz Fourier frequency without the use of cryogenics, and was limited by the thermal noise in the microwave interferometer. To facilitate tuning and locking, an automatically balanced microwave frequency discriminator was developed using voltage-controlled attenuators and phase shifters. Rapid frequency tuning of the oscillator was achieved by varying the interferometer phase mismatch and automatically controlling the carrier suppression without tuning the high-Q resonator.**

***Index Terms*—Effective noise temperature, frequency discriminator, microwave interferometer, phase and amplitude fluctuations.**

I. Introduction

THE frequency discriminator is a key part of any oscillator frequency-stabilization system and improvement of its sensitivity results in the corresponding improvement in the oscillator phase noise. The ideas of using a carrier–suppression technique for improving the sensitivity of frequency discriminators can be found in literature dating back to the late 1950's [1]. In particular, a carrier–rejection filter based on a critically coupled microwave resonator in reflection was suggested in [2] as the dispersive element in a frequency discriminator. By following this work, Santiago and Dick developed a cryogenic X-band frequency discriminator with an extremely low phase-noise floor of -160 dBc/Hz at Fourier frequency $f = 1$ kHz in 1992 [3], [4]. This performance was achieved by using a sapphire loaded cavity (SLC) resonator operating at liquid-nitrogen temperature. However, the sensitivity of Santiago and Dick's frequency discriminator was limited by the lack of carrier suppression caused by nonperfect matching of the cavity to the transmission line. The drawbacks of frequency discriminators based on the critically coupled resonators were overcome in the interferometric measurement systems developed at the University of Western Australia, Nedlands, W.A., in the mid-1990's, and is subject to international patent [5]–[9]. By implementing the interferometric signal processing, the phase-noise floor of an X-band frequency discriminator was reduced to a level of -155 dBc/Hz at 1-kHz Fourier frequency without the use of cryogenics. This has enabled the development of a 9-GHz oscillator with the phase-noise spectral density of -150 dBc/Hz at $f = 1$ kHz, which represented at least a 25-dB improvement in the oscillator phase-noise performance as compared with the previous state-of-the-art [10], [11].

The enhanced sensitivity of the interferometric measurement system arises from its ability to satisfy two seemingly contradictory requirements: having high power at the input of the interferometer, and enabling the small-signal operation of a microwave readout system, which represents a homodyne downconvertor for converting fluctuations of the microwave signal at the output of interferometer into voltage noise. The low-noise operation of the readout system is achieved by balancing the interferometer and amplifying the signal with the suppressed carrier by using a high-gain low-noise microwave amplifier before processing it in the nonlinear mixing stage. The combination of carrier suppression and a low-noise microwave amplification enables the interferometric noise-measurement system to operate with effective noise temperatures close to its physical temperature [5].

In this paper, we consider: 1) the principles of operation of interferometric frequency discriminators and the noise mechanisms affecting their sensitivity; 2) the applications of microwave interferometric signal processing to phase-noise reduction in microwave oscillators; and 3) noise analysis and performance of tunable ultra-low phase-noise oscillators with automatic carrier suppression.

II. Phase-Noise Floor of the Interferometric Frequency Discriminator

The schematic diagram of the interferometric frequency discriminator is shown in Fig. 1. The key part of the discriminator is a microwave interferometer with a high-Q resonator in one of its arms. The sensitivity of the interferometric frequency discriminator to pump oscillator frequency fluctuations results from frequency-to-phase conversion, which takes place in the high-Q resonator. This upsets the balance of the interferometer and results in power fluctuations at its output. The signal with suppressed carrier from the output of interferometer is

Manuscript received November 20, 1997; revised May 15, 1998. This work was supported by the Australian Research Council and Poseidon Scientific Instruments Pty. Ltd., Fremantle, W.A.

The authors are with the Physics Department, University of Western Australia, Nedlands 6907, W.A.

Publisher Item Identifier S 0018-9480(98)06726-X.

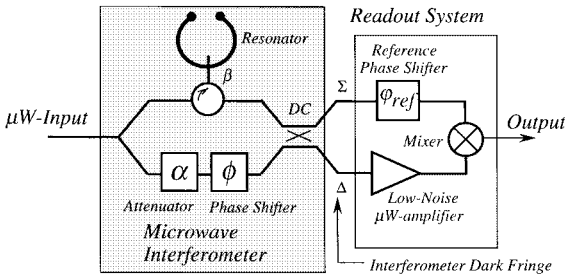

Fig. 1. An interferometric frequency discriminator.

processed by the homodyne phase-sensitive readout system, which is formed by the low-noise microwave amplifier, reference phase shifter, and double-balance mixer. The microwave amplifier is introduced in front of the mixer in order to take advantage of the carrier suppression and override the mixer's high effective noise temperature. While operating in the small-signal regime, the effective noise temperature of the microwave readout system is constant, and not affected by the flicker noise of microwave amplifier. This allows the phase sensitivity of the interferometric frequency discriminator to be increased by increasing the power incident on the high-Q resonator as long as the carrier suppression remains sufficient.

A number of noise mechanisms, both intrinsic and external with respect to the frequency discriminator, limit its sensitivity and, therefore, introduce uncertainty in the process of oscillator frequency measurements. One of these mechanisms can be described in terms of the readout-system effective noise temperature $T_{\rm RS}$, which can be expressed as a sum of three components representing noise contributions of the microwave-amplifier, double-balance mixer, and lossy components of the interferometer

$$T_{\rm RS} = T_{\rm amp}^{\rm eff} + T_{\rm mix}^{\rm eff}/K_{\rm amp} + T_o. \tag{1}$$

Here, $K_{\rm amp}$ and $T_{\rm amp}^{\rm eff}$ are the microwave-amplifier gain and effective noise temperature, respectively, and T_o is the ambient temperature. High amplifier gain makes the mixer noise contribution insignificant, and (1) can be simplified to $T_{\rm RS} = T_{\rm amp}^{\rm eff} + T_o$.

In the general case, $T_{\rm RS}$ is a function of Fourier frequency f and power at the input of the low-noise microwave amplifier $P_{\rm amp}$. This dependence is caused by the microwave-amplifier flicker noise, which intensity scales proportionally with input power [12], [13]. For a typical microwave amplifier, we found that [5]

$$T_{\rm RS} = T_{\rm RS}^{\rm min}(1 + f_c/f)^2. \tag{2}$$

Here, $T_{\rm RS}^{\rm min}$ is the minimum effective noise temperature of the readout system measured with a 50-Ω termination attached to its input, and f_c is the flicker-noise corner frequency given by

$$f_c({\rm Hz}) = 1.5 * 10^6 * P_{\rm amp}({\rm mW}). \tag{3}$$

By suppressing the carrier at the output of the interferometer and choosing a microwave amplifier with a low level of Johnson noise, the readout-system effective noise temperature can be reduced to a level close to the ambient temperature T_o. For instance, the effective noise temperature of about 360 K was measured at $P_{\rm amp} \leq -40$ dBm [5]. The value of $T_{\rm RS}$ being close to T_o implies that the measurement-system noise floor is primarily limited by thermal fluctuations in the lossy components of the interferometer.

Assuming that the oscillator operating frequency $f_{\rm osc}$ is equal to the resonant frequency of the high-Q resonator $f_{\rm res}$, the interferometric frequency-discriminator phase-noise floor in terms of one-sided spectral densities is given by [5]

$$\mathcal{L}_\varphi^{FD(1)}(f) = \frac{k_B T_{\rm RS}}{P_{\rm inc}} \frac{(1+\beta)^2}{4\beta^2} \left\{1 + (\Delta f_{0.5}^{(L)}/f)^2\right\}. \tag{4}$$

Here, $P_{\rm inc}$ is the power of microwave signal incident on the resonator, k_B is Boltzman's constant, β is the resonator coupling coefficient, $f_{\rm res}$ and Q_o are the resonant frequency and unloaded Q-factor of the resonator, respectively, and $\Delta f_{0.5}^{(L)} = f_{\rm res}(1+\beta)/2Q_o$ is the resonator loaded half-bandwidth. Substituting into (4) the set of parameters corresponding to a typical room temperature SLC, $\beta = 0.7$, $Q_o = 190\,000$, $f_{\rm res} = 9$ GHz, and assuming that $T_{\rm RS} = 360$ K and $P_{\rm inc} = 50$ mW, we calculate a one-sided phase-noise floor of -155 dBc/Hz at $f = 1$ kHz. This is more than 50 dB better than the phase noise of a free-running oscillator based on the same resonator [6], and illustrates the high potential of the interferometric phase-noise reduction technique.

Another component of the frequency-discriminator phase-noise floor is due to the phase modulation (PM) and amplitude modulation (AM) fluctuations inside the microwave interferometer. These fluctuations occur in voltage-controlled and ferrite components of the interferometer, and can also be vibrationally induced. Assuming that $f_{\rm osc} = f_{\rm res}$, the frequency-discriminator phase-noise floor due to the above mechanism is given by

$$\mathcal{L}_\varphi^{FD(2)}(f) \approx \left[\mathcal{L}_\varphi^{\rm int}(f) + \mathcal{L}_{\rm AM}^{\rm int}(f)\,\delta\varphi_{\rm ref}^2\right] \frac{(1-\beta)^2}{4\beta^2} \cdot\left\{1 + (\Delta f_{0.5}^{(L)}/f)^2\right\}. \tag{5}$$

Here, $\mathcal{L}_\varphi^{\rm int}(f)$ and $\mathcal{L}_{\rm AM}^{\rm int}(f)$ are spectral densities of phase and amplitude fluctuations in the interferometer, respectively, and $\delta\varphi_{\rm ref}$ is the error in setting the reference phase shift, which results in a residual sensitivity of the frequency discriminator to amplitude fluctuations in the interferometer. Using the above parameters of the SLC resonator and considering the noise performance of typical voltage-controlled devices [7], we can show that $\mathcal{L}_\varphi^{FD(2)} = -141$ dBc/Hz at $f = 1$ kHz. This is 14 dB higher than the thermal noise floor calculated earlier from (4). Removing the voltage-controlled devices from the interferometer leaves the microwave circulator as the only source of nonthermal fluctuations inside the interferometer (see Fig. 1), and allows a significant reduction in the frequency-discriminator noise floor. Using the phase-noise model of a single isolator [7], [8]

$$\mathcal{L}_\varphi^{\rm ISL}(F) \approx -150 - 12\log_{10}(F)\ {\rm dBc/Hz} \tag{6}$$

from (5) it follows $\mathcal{L}_\varphi^{FD(2)}(1\ {\rm kHz}) = -158$ dBc/Hz, which is lower than the noise floor calculated from (4). However,

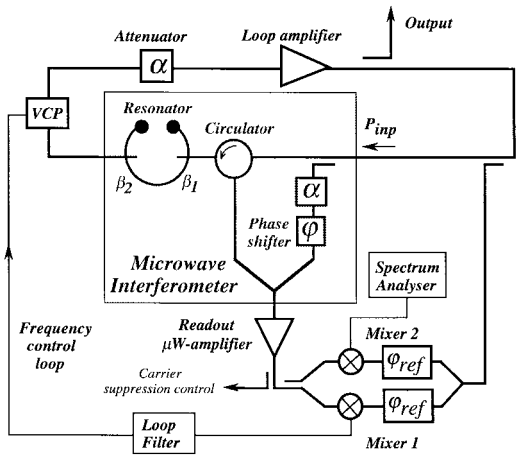

Fig. 2. A frequency-stabilized microwave oscillator with interferometric signal processing.

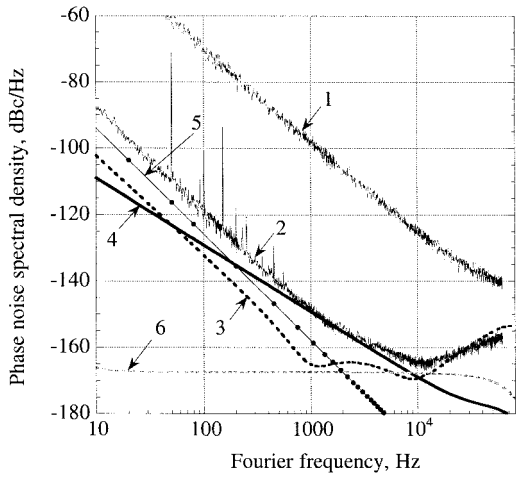

Fig. 3. Phase-noise performance of a 9-GHz oscillator. Curve 1: measured phase noise of the free-running oscillator. Curve 2: measured phase noise of frequency-stabilized oscillator. Curve 3: phase noise due to the frequency-servo finite-loop gain. Curve 4: phase noise due to readout-system effective noise temperature. Curve 5: phase noise due to intrinsic phase fluctuations of microwave circulator. Curve 6: phase noise due to oscillator amplitude fluctuations.

at low Fourier frequencies, the circulator noise contribution becomes the dominant factor and determines the frequency-discriminator noise floor. This is because the $\mathcal{L}_{\varphi}^{FD(2)}$ increases as $1/f^3$ while $\mathcal{L}_{\varphi}^{FD(1)} \sim 1/f^2$.

When the oscillator operating frequency $f_{\rm osc}$ is not exactly equal to $f_{\rm res}$, the phase noise of the interferometric frequency discriminator is affected by the oscillator AM noise. The numerical estimate for the frequency-discriminator phase-noise floor due to this effect is approximately -160 dBc/Hz at $f =$ 1 kHz, assuming that $f_{\rm osc} - f_{\rm res} = 2$ kHz and the oscillator AM noise spectral density $\mathcal{L}_{\rm AM}^{\rm osc}(1\ {\rm kHz}) = -140$ dBc/Hz. Another mechanism for the amplitude-to-phase conversion in an interferometric frequency discriminator is related to the error in setting the reference phase shift $\delta\varphi_{\rm ref}$. The frequency-discriminator phase-noise floor due to this effect is given by

$$\mathcal{L}_{\varphi}^{FD(3)}(f) = \mathcal{L}_{\rm AM}^{\rm osc}(f)\tan^2(\delta\varphi_{\rm ref}). \tag{7}$$

Equation (7) allows the upper limit on the reference phase-shift error to be calculated. Thus, assuming an oscillator AM noise of $\mathcal{L}_{\rm AM}^{\rm osc}(1\ {\rm kHz}) \approx -120$ dBc/Hz, the phase error $\delta\varphi_{\rm ref}$ must be kept less than 1.4° if the thermal-noise limited performance given by (4) is to be achieved.

III. Ultra-Low Phase-Noise Oscillator with Interferometric Signal Processing

A simplified diagram of the frequency-stabilized microwave oscillator with interferometric signal processing is shown in Fig. 2. The high-Q resonator is used both as a bandpass filter in the loop oscillator and a dispersive element of the frequency discriminator [14]. The oscillator phase-noise suppression is achieved by applying a filtered signal from the output of the frequency discriminator to the voltage-controlled phase shifter (VCP) inside the loop oscillator. The VCP allows the tuning of the oscillator operating frequency by changing the effective electric length of the loop. The frequency discriminator and VCP represent the sensor and actuator, respectively, of a frequency-control system, which locks the oscillator to a selected resonant mode of the high-Q resonator. An auxiliary channel of the readout system based on Mixer 2 (see Fig. 2) allows *in situ* monitoring of the noise performance of the readout microwave amplifier.

The spectral density of the oscillator phase noise at Fourier frequencies within the bandwidth of a high-gain frequency-control system is given by [5]

$$\mathcal{L}_{\varphi}^{\rm osc}(f) = \sum_j \mathcal{L}_{\varphi}^{FD(i)}(f) + \frac{\mathcal{L}_f^{\rm res}(f)}{f^2} \tag{8}$$

where the first term represents the frequency-discriminator phase-noise floor due to the noise mechanisms discussed earlier, and the second term represents the high-Q resonator resonant frequency fluctuations. Such fluctuations arise from various effects including temperature, and seismic and radiation pressure fluctuations [15].

The phase noise of the 9-GHz loop oscillator with the interferometric frequency discriminator was measured by using a second interferometric frequency discriminator with similar sensitivity. Both frequency discriminators were based on the commercial temperature-stabilized SLC's developed by Poseidon Scientific Instruments Pty Ltd., Fremantle, W.A. The results of noise measurements are shown in Fig. 3. Curve 1 in Fig. 3 corresponds to the phase noise of the free-running loop oscillator. Closing the frequency feedback loop with a dc gain of 58 dB reduces the oscillator phase noise by 50 dB at Fourier frequencies below a few kilohertz (curve 2). The one-sided phase noise of the oscillator in this case follows a flicker-frequency law and fits to

$$\mathcal{L}_{\varphi}^{\rm osc}(f) = -60 - 30\log_{10}(f)\ {\rm dBc/Hz}. \tag{9}$$

which corresponds to $\mathcal{L}_{\varphi}^{\rm osc}(1\ {\rm kHz}) \approx -150$ dBc/Hz. The various components of the oscillator phase noise given by

curves 3–6 in Fig. 3 were calculated from a small-signal model of the low-noise oscillator. Here, we assumed the following parameters:

1) power incident on the SLC resonator $P_{\rm inc} = 50$ mW;
2) reference phase-shift error $\delta\varphi_{\rm ref} = 3°$;
3) oscillator AM noise spectral density $S_{\rm AM}^{\rm osc}(1\ {\rm kHz}) \approx -140$ dBc/Hz;
4) 60-dB level of carrier suppression.

It was also assumed that the carrier is suppressed at the SLC resonant frequency and the total dc gain of the feedback control loop was equal to 58 dB. The loop filter was designed to provide a phase margin of the open-loop transfer function equal to 25°.

Curve 3 shows the suppression of the free-running oscillator phase noise by the frequency servo. This level of the oscillator phase noise could be achieved if the frequency discriminator was noiseless. Comparing curves 2 and 3 shows that the relative degradation of the oscillator phase noise at Fourier frequencies above 10 kHz is due to the insufficient gain of the frequency servo. Curve 4 in Fig. 3 corresponds to the oscillator phase noise due to the readout-system effective noise temperature. It varies as $1/F^2$ and is a major factor limiting the oscillator phase-noise performance at Fourier frequencies from 200 Hz to 10 kHz. At low Fourier frequencies $f < 200$ Hz, the oscillator phase noise is limited by phase fluctuations in the circulator (curve 5 in Fig. 3). The phase-noise performance of the oscillator in this frequency range can be improved by setting the resonator coupling close to critical ($\beta_{\rm eq} \rightarrow 1$) (5). The same goal can also be achieved by replacing the circulator with a 3-dB hybrid coupler, as suggested in [4]. In this case, the power at the input of the microwave interferometer must be increased by 6 dB to compensate for the loss of signal power in the hybrid coupler. The overall phase noise of such an oscillator at Fourier frequencies 50 Hz $< f <$ 5 kHz is entirely determined by the readout-system effective noise temperature (curve 4 in Fig. 3). The component of the oscillator phase noise caused by AM-to-PM conversion (7) is shown by curve 6 in Fig. 3.

From the above discussion, it follows that further improvements in the oscillator phase-noise performance could be achieved by increasing both the power incident on the resonator and its Q-factor. For instance, a phase-noise spectral density of the order of $\mathcal{L}_{\varphi}^{\rm osc}(1\ {\rm kHz})$ is expected for the room temperature SLC oscillator operating with an incident power of $P_{\rm inc} = 500$ mW. To increase the Q-factor of the SLC, it must be cooled to cryogenic temperatures. Q-factors of order $5 \cdot 10^7$ and $5 \cdot 10^9$ have been achieved for the SLC resonators operating at liquid nitrogen (77 K) and helium (4.2 K) temperatures, respectively [16], [17]. The phase noise of a frequency-stabilized oscillator based on a 77-K SLC resonator with $P_{\rm inc} = 50$ mW is expected to be equal to -180 dBc/Hz at $f = 1$ kHz. It is worth noting that at Fourier frequencies higher than the resonator bandwidth, the oscillator phase noise does not depend on the Q-factor [see (4) and (5)]. This implies that at $f \geq 250$ Hz, the phase noise of the cryogenic oscillator based on the 77-K SLC resonator will not be affected by cooling to lower temperatures.

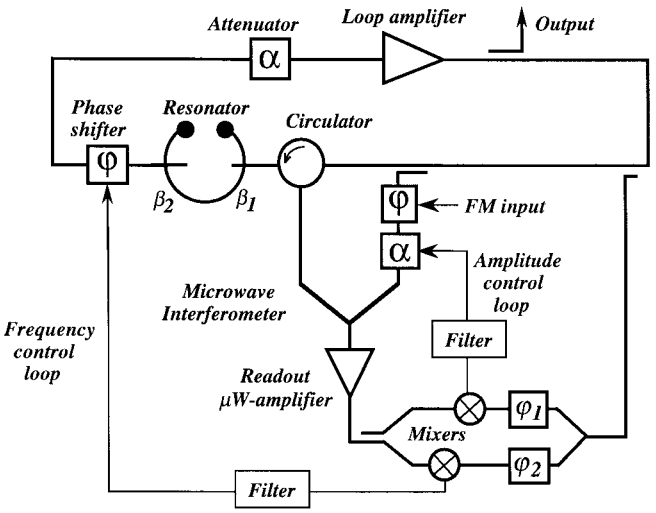

Fig. 4. A frequency-stabilized microwave oscillator with automatic carrier suppression.

IV. Tunable Ultra-Low Phase-Noise Oscillator with Automatic Carrier Suppression

A. Principle of Operation

The optimal phase-noise performance of the above oscillator is achieved at frequencies close to the resonant frequency of the high-Q resonator. Tuning the operating frequency of such an oscillator (by changing the phase balance of the interferometer) ruins the carrier suppression and degrades the oscillator phase-noise performance due to flicker noise in the readout amplifier. To minimize the degradation of the oscillator phase noise, an automatic carrier–suppression system capable of maintaining the balance of the interferometer within the oscillator tuning range has been developed. The general configuration of the microwave oscillator with an automatic carrier–suppression system is shown in Fig. 4. In such an oscillator, the carrier is automatically suppressed due to the joint operation of two feedback control systems. The first (frequency) control system maintains the phase balance of the interferometer, while the second one (amplitude-control system) keeps the amplitude mismatch between the interferometer arms at a minimum. The sensors of both control systems are almost identical, except for the quadrature settings of the reference phase shifters $\varphi_{\rm ref1}$ and $\varphi_{\rm ref2}$. In practice, the optimal values of the reference phase shifts are sought at frequency close to $f_{\rm res}$ to ensure the optimal sensitivity of each sensor and minimum cross coupling between the control systems. The values of $\varphi_{\rm ref1}$ and $\varphi_{\rm ref2}$ obtained in the process of such optimization remain unchanged during the oscillator frequency tuning.

Responding to variations of interferometer phase mismatch, the two feedback control systems alter the oscillator frequency and the attenuation of the interferometer compensating arm until the balance of the interferometer at a new operating frequency is achieved. This enables the degradation of the oscillator phase noise associated with the lack of carrier suppression to be completely avoided. However, there are other noise mechanisms which effect the oscillator phase

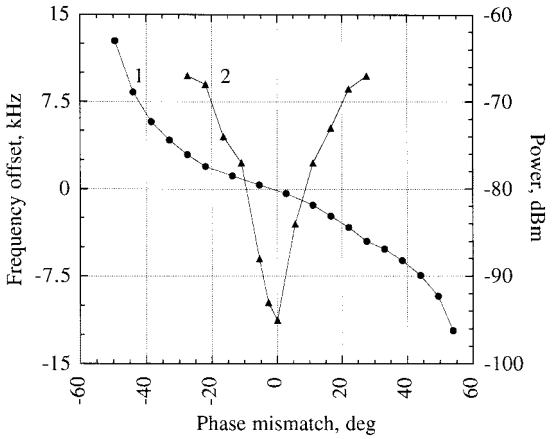

Fig. 5. Oscillator frequency offset from the resonant frequency of SLC resonator (curve 1) and power at the output of microwave interferometer (curve 2) as functions of interferometer phase mismatch.

noise and depend only on the oscillator frequency shift from the high-Q resonator center of resonance $f_{\rm osc} - f_{\rm res}$, and is discussed in the following section.

The tuning range of the frequency-stabilized oscillator with automatic carrier suppression is limited by the maximum phase mismatch $\Delta\Psi_{\max}$ at which the interferometer can still be balanced. For a two-port high-Q resonator, the value of $\Delta\psi_{\max}$ is given by

$$\Delta\Psi_{\max} = a\sin(\beta_{\rm eq}) \tag{10}$$

where $\beta_{\rm eq}$ is the equivalent coupling of the high-Q resonator equal to $\beta_{\rm eq} = \beta_1/(1+\beta_2)$, and β_1 and β_2 are the resonator coupling coefficients. Here, it is assumed that $\beta_{\rm eq} < 1$. The value of $\Delta\Psi_{\max}$ corresponds to the maximum phase deviation of the cavity reflection coefficient with frequency. From (10), the boundaries of the oscillator frequency tuning range can be calculated to be

$$f_{\rm osc} = f_{\rm res} \pm \Delta f_{0.5}\sqrt{1-\beta_{\rm eq}^2} \tag{11}$$

where $\Delta f_{0.5} = (f_{\rm res}/2Q_o)(1+\beta_2)$ is the resonator half-bandwidth and Q_0 is the unloaded Q-factor.

The experimental dependence of oscillator operating frequency on phase mismatch is shown in Fig. 5 (curve 1). It corresponds to the oscillator based on a typical room-temperature SLC resonator having the following parameters:

1) $f_{\rm res} = 9$ GHz;
2) $\beta_1 = 0.75$, $\beta_2 = 0.15$;
3) $Q_0 = 200\ 000$.

From Fig. 5, it follows that the frequency is a nonlinear function of the phase mismatch, and the total tuning range is approximately ± 14 kHz, which is comparable to the SLC resonator half-bandwidth $\Delta f_{0.5}$. From (11), it follows that the oscillator tuning range can be increased by reducing the resonator's Q-factor and its coupling coefficient. However, this will be achieved at the expense of degrading the oscillator phase noise [see (4) and (5)]. This confirms the intuitive perception that low-phase-noise operation and broad frequency tuning are mutually exclusive.

Power at the output of microwave interferometer (input of low-noise microwave amplifier) as a function of phase mismatch is shown by curve 2 in Fig. 5. This dependence corresponds to when the frequency and amplitude-control systems are both operating. It shows that even at the boundaries of the tuning range, the power at the input of the low-noise microwave amplifier does not exceed -68 dBm, which is low enough not to cause any significant degradation of the frequency-discriminator effective noise temperature [see (2) and (3)]. These experiments have also confirmed that extremely high levels of carrier suppression could be reproducibly achieved and maintained. Defining the carrier suppression as a ratio of power incident on the high-Q resonator to the power at the input of the microwave readout amplifier—$cs = P_{\rm inc}/P_{\rm amp}$—and applying this definition to the experimental data in Fig. 5, a maximum value of cs equal to 109 dB was obtained.

B. Oscillator Small-Signal Model

The noise performance of a microwave oscillator with automatic carrier suppression is analyzed by solving a system of coupled nonlinear differential equations, which describe the joint operation of frequency and amplitude-control systems. The first characteristic equation of this system corresponds to the loop oscillator in which the total phase shift around the loop θ is adjusted by the error signal from the frequency discriminator. Expressing the operating frequency of the loop oscillator as a function of the phase shift θ [18]

$$\Delta f_{\rm osc} = f_{\rm res} + \Delta f_{0.5}^{(L)}\tan\theta \tag{12a}$$

and taking into account that the θ is a function of the output voltage of the filter in the frequency control system, results in

$$\Delta f_{\rm osc} = \Delta f_{0.5}^{(L)}\tan\{\theta_o + \theta[U_o + K_F(p)U_{\rm FD} \cdot(\Delta f_{\rm osc}, \Delta m, \Delta\psi, \cdots)]\} \tag{12b}$$

where $\Delta f_{\rm osc} = f_{\rm osc} - f_{\rm res}, \theta_o$ is a voltage independent component of the loop oscillator phase shift, U_o is an initial bias voltage of the electronic phase shifter, $K_F(p)$ is the differential operator corresponding to the frequency control system filter transfer function, and $U_{\rm FD}$ is the frequency discriminator output voltage The latter is a function of frequency offset $\Delta f_{\rm osc}$, interferometer phase and amplitude mismatches $\Delta\psi$ and Δm, respectively, power incident on the high-Q resonator $P_{\rm inc}$, the gain of microwave amplifier $K_{\rm amp}$, and some other parameters.

The characteristic equation of the amplitude-control system is derived by "traveling" around the control loop and combining the transfer functions of all its elements. Starting from the voltage-controlled attenuator in the compensating arm of the interferometer, its attenuation can be expressed as a nonlinear function of the applied voltage $U_{\rm vca}$

$$\alpha = \alpha(U_{\rm vca}). \tag{13a}$$

Representing $U_{\rm vca}$ as a sum of the dc bias voltage V_o and the amplitude-discriminator filtered voltage, the following

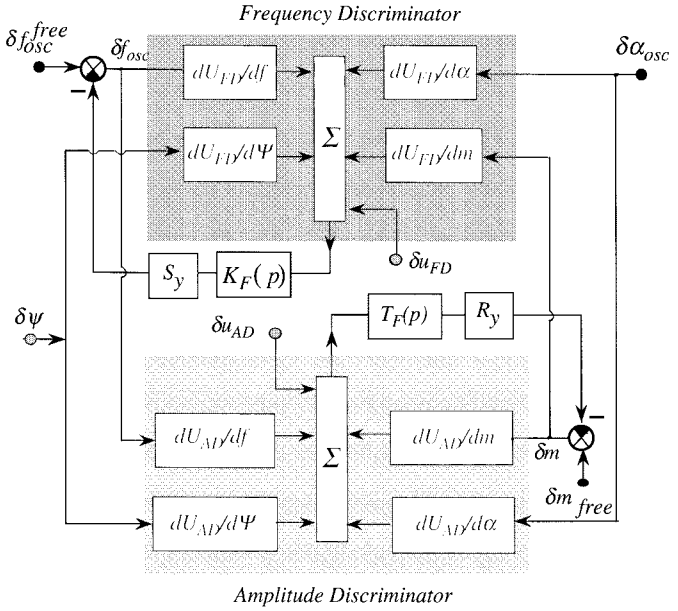

Fig. 6. The small-signal model of a frequency-stabilized microwave oscillator with automatic carrier suppression.

characteristic equation of the amplitude-control system is obtained:

$$\frac{\Delta m = \alpha[V_o + T_F(p)U_{\rm AD}(\Delta f_{\rm osc}, \Delta m, \Delta\psi, \cdots)]}{\alpha_o} \quad (13b)$$

where $T_F(p)$ is the filter-transfer function and $U_{\rm AD}$ is the amplitude-discriminator output voltage. The parameter α_o in (13b) is the optimal attenuation of the compensating arm of the interferometer, which can be found from the condition of carrier suppression: $\alpha_o = |\Gamma(\tilde{f}_{\rm res})|$, where Γ is the reflection coefficient of the high-Q resonator at some arbitrary frequency $\tilde{f}_{\rm res}$, which is not necessarily equal to $f_{\rm res}$.

By linearizing the system of characteristic equations (12b) and (13b) in the vicinity of the stationary regime, one can obtain a set of differential equations, which are linear with respect to small fluctuations of the oscillator operating frequency $\delta f_{\rm osc}$ and interferometer amplitude mismatch δm. Presenting these equations in a graphical form yields a block diagram, shown in Fig. 6, which will be referred to as an oscillator small-signal model. The graphical approach simplifies the understanding of the oscillator noise analysis by visualizing the interaction between two control systems and allowing one to trace the effect of various noise sources on the oscillator frequency stability. From the small-signal model of the oscillator, it is also clear that the cross-coupling between the two control systems is caused by residual sensitivities of both discriminators to the unwanted type of fluctuations. Thus, in general, the frequency discriminator is sensitive to AM fluctuations in the interferometer, while the amplitude discriminator exhibits some sensitivity to oscillator phase noise. It should be noted that the sensitivities of both frequency and amplitude discrimination are functions of the interferometer phase mismatch $\Delta\psi$ and, therefore, vary in the process of frequency tuning. Assuming that both control systems are operating, the sensitivities of frequency discriminator to phase fluctuations inside the interferometer $dU_{\rm FD}/d\psi$ and oscillator

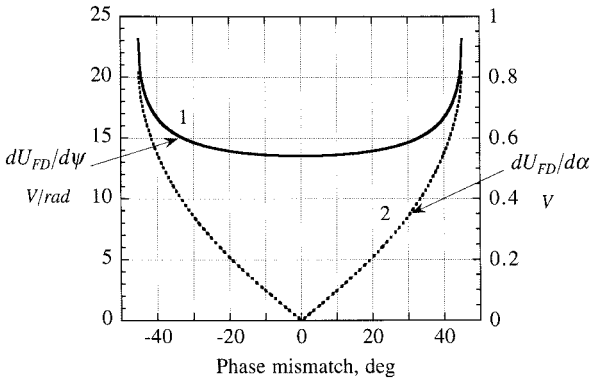

Fig. 7. The frequency-discriminator sensitivities to phase fluctuations inside interferometer (curve 1) and oscillator amplitude noise (curve 2) as functions of interferometer phase mismatch. Both control systems are operational.

AM noise $dU_{\rm FD}/d\alpha$ have been calculated as functions of the $\Delta\psi$. The results of these calculations are shown in Fig. 7 (curves 1 and 2, respectively). They imply that oscillator phase-noise performance degrades near the boundaries of the tuning range as both $dU_{\rm FD}/d\psi$ and $dU_{\rm FD}/d\alpha$ rapidly increase as $\Delta\psi \rightarrow \pm\Delta\psi_{\max}$.

The major disturbances affecting the oscillator frequency stability include: 1) frequency fluctuations of the free-running oscillator $\delta f_{\rm osc}^{\rm free}$ caused primarily by phase fluctuations of the microwave amplifier in the loop oscillator; 2) phase $\delta\psi$ and amplitude $\delta m_{\rm free}$ fluctuations inside the interferometer; 3) oscillator amplitude fluctuations $\delta\alpha_{\rm osc}$; and 4) intrinsic voltage fluctuations $\delta u_{\rm FD}$ and $\delta u_{\rm AD}$ at the output of frequency and amplitude discriminators. Most of these fluctuations are statistically independent, except for the last two ($\delta u_{\rm FD}$ and $\delta u_{\rm AD}$), which are strongly correlated, as they are primarily caused by the same factor—thermal noise at the input of the microwave readout amplifier (see Fig. 4).

The fluctuations of the oscillator operating frequency due to the above disturbances can be found by using the oscillator small-signal model. We consider below only two noise mechanisms causing the oscillator frequency fluctuations. The first mechanism is associated with fluctuations $\delta f_{\rm osc}^{\rm free}$. It imposes the following limit on frequency fluctuations of the frequency-stabilized oscillator:

$$\delta f_{\rm osc}^{(f)} = \delta f_{\rm osc}^{\rm free}/(1+\tilde{\gamma}) \quad (14)$$

where

$$\tilde{\gamma} = \gamma[1 - \xi\gamma_a/(1+\gamma_a)] \quad (15)$$

is the modified open-loop gain of the frequency-control system. This is an important parameter, as it allows the stability analysis of the stationary regime of the tunable oscillator to be performed. It also shows how well the frequency fluctuations of the free-running oscillator are suppressed by the frequency-control system. Parameters γ, γ_a in (15) are the open-loop gains of the frequency and amplitude-control systems, respectively, given by

$$\gamma = (dU_{\rm FD}/df)K_F(p)S_y$$

and

$$\gamma_a = (dU_{\rm AD}/dm)T_F(p)S_a \quad (16)$$

where $dU_{\rm FD}/df$ is the sensitivity of frequency discriminator to frequency fluctuations, $dU_{\rm AD}/dm$ is the sensitivity of amplitude discriminator to AM fluctuations inside the interferometer, and S_y and S_a are transfer functions of actuators of frequency and amplitude-control systems, respectively. They are given by

$$S_y = (d\theta/du)\{\Delta f_{0.5}^{(L)}/\cos^2(\theta_{\rm stat}) + p\}$$

and

$$S_a = (1/\alpha_o)\,\frac{d\alpha}{dU_{\rm vca}} \tag{17}$$

where $\theta_{\rm stat}$ is the stationary value of the loop phase shift, and $d\theta/du$ and $d\alpha/dU_{\rm vca}$ are the voltage derivatives taken at the point of stationary regime. Parameter ξ in (15) is a coefficient characterizing coupling between two servo control systems and are given by

$$\xi = \frac{\partial U_{\rm FD}/\partial m}{\partial U_{\rm FD}/\partial f}\,\frac{\partial U_{\rm AD}/\partial f}{\partial U_{\rm AD}/\partial m} \tag{18}$$

where $dU_{\rm AD}/df$ is the sensitivity of amplitude discriminator to oscillator frequency fluctuations, and $dU_{\rm FD}/dm$ and $dU_{\rm AD}/dm$ are the respective sensitivities of frequency and amplitude discriminators to interferometer AM mismatch fluctuations.

The second noise mechanism causing the oscillator frequency fluctuations is related to fluctuations of the interferometer phase mismatch $\delta\psi$. The limit imposed on the $\delta f_{\rm osc}$ by this mechanism is given by

$$\delta f_{\rm osc}^{(\psi)} = \delta\psi\,\frac{\gamma}{1+\tilde{\gamma}} \cdot\left\{\frac{dU_{\rm FD}/d\psi}{dU_{\rm FD}/df} + \frac{\gamma_a}{1+\gamma_a}\,\frac{dU_{\rm FD}/dm}{dU_{\rm FD}/df}\,\frac{dU_{\rm AD}/d\psi}{dU_{\rm AD}/dm}\right\} \tag{19}$$

where $dU_{\rm FD}/d\psi$ and $dU_{\rm AD}/d\psi$ are the respective sensitivities of frequency and amplitude discriminators to phase fluctuations inside the interferometer $\delta\psi$. For the spectral components of $\delta\psi$ within the bandwidth of the frequency-control system, but outside the bandwidth of the amplitude control one, (17) may be simplified as

$$\delta f_{\rm osc}^{(\psi)} = \delta\psi\,\frac{dU_{\rm FD}/d\psi}{dU_{\rm FD}/df} = d\psi\,\frac{df}{d\Psi} \tag{20}$$

where $df/d\psi$ is the gradient of oscillator frequency dependence on the phase mismatch $f(\Psi)$. An example of such dependence measured for the SLC-based oscillator is shown in Fig. 5 (curve 1). The shape of $f(\Psi)$ indicates that sensitivity of oscillator frequency to phase mismatch fluctuations increases at the boundaries of the tuning range.

C. Oscillator Phase-Noise Performance

The results of noise analysis of the tunable oscillator are presented in Fig. 8. By using the oscillator small-signal model, various components of the oscillator phase noise were calculated as functions of Fourier frequency (curves 2–6). To verify the results of numerical simulations, the measured phase-noise spectrum of the tunable oscillator is also shown in Fig. 8 (curve 1). For the sake of generality, both numerical and theoretical data were obtained for the oscillator operating at 10-kHz offset from the SLC center of resonance. The simulations were performed assuming the same set of parameters specified earlier in Section III. It was also assumed that the AM noise of the voltage-controlled attenuator in the compensating branch of the interferometer was equal to $\mathcal{L}_{\rm AM}^{\rm vca} \approx -150$ dBc/Hz [7]. Fluctuations of the interferometer phase mismatch were taken in a form $\mathcal{L}_{\varphi}^{\rm int}(f) = 10^{-14}/f$ dBc/Hz [7]. The open-loop dc gains of the frequency and amplitude-control systems were chosen to be equal to 55 and 50 dB, respectively. Curve 2 in Fig. 8 shows the suppression of the free-running oscillator phase noise by the frequency servo. This level of the oscillator phase noise could be achieved if the frequency discriminator was noiseless. Curve 3 gives the oscillator phase-noise floor due to phase fluctuations inside the microwave interferometer. It varies as $1/f^3$ and is a major factor limiting the oscillator phase noise at offset frequencies below 400 Hz. As was mentioned previously, this noise floor can be reduced by setting the resonator coupling close to critical ($\beta \to 1$) at a given value of a resonator Q-factor. Curve 4 corresponds to the oscillator phase-noise floor imposed by the finite effective noise temperature of the microwave readout system $T_{\rm eff}$. It varies like $1/f^2$ within the frequency range from 100 Hz to 10 kHz and like $1/f^4$ at $f \le 10$ Hz. The rapid increase of the oscillator noise at $f \le 10$ Hz is caused by the lack of carrier suppression [see Fig. 6 and (2) and (3)]. At high offset frequencies around 10 kHz, the oscillator phase noise is limited by oscillator AM noise (curve 5 in Fig. 8). This limit arises from the residual sensitivity of the frequency discriminator to oscillator AM noise when $f_{\rm osc} \neq f_{\rm res}$. The last component of the oscillator phase-noise floor is due to AM fluctuations inside the interferometer (curve 6 in Fig. 8). This noise floor was calculated for the amplitude-control system based on the single-pole low-pass filter with corner frequency 10 Hz, which was used in our experiments. By increasing either

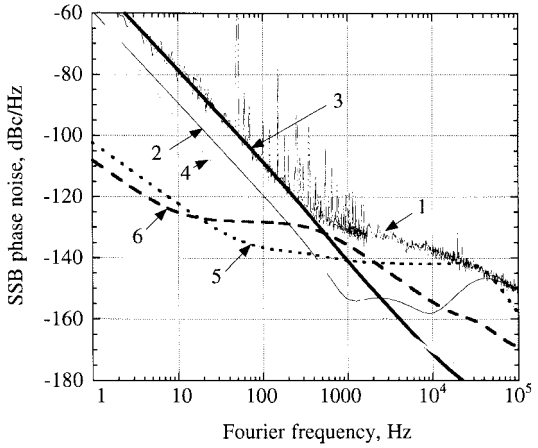

Fig. 8. The noise budget of frequency-stabilized microwave oscillator with automatic carrier suppression. Curve 1: measured phase noise. Curve 2: noise floor due to the limited gain of frequency servo. Curve 3: noise floor due to phase fluctuations inside interferometer. Curve 4: noise floor due to readout-system finite noise temperature. Curve 5: noise floor due to oscillator AM noise. Curve 6: noise floor due to amplitude fluctuations inside interferometer. It is assumed that $f_{\rm osc} - f_{\rm res} = 10$ kHz.

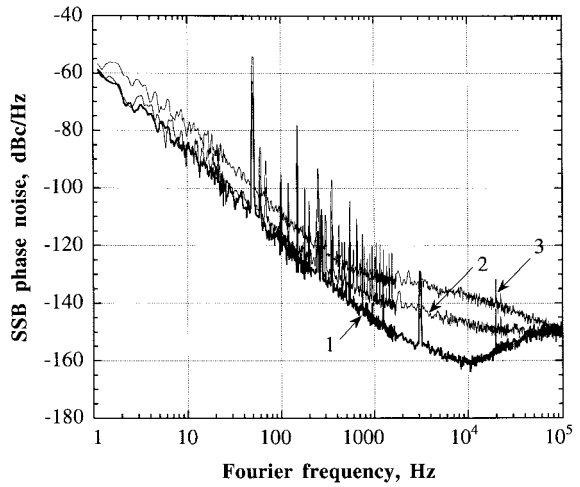

Fig. 9. The phase-noise spectra of a frequency-stabilized microwave oscillator with automatic carrier suppression at different offsets from the resonant frequency of the SLC resonator. Curve 1: $f_{\rm osc} = f_{\rm res}$ Curve 2: $f_{\rm osc} = f_{\rm res} + 5$ kHz. Curve 3: $f_{\rm osc} = f_{\rm res} + 10$ kHz.

the bandwidth of the amplitude-control system or its gain, the effect of this noise source on the oscillator phase-noise performance can be reduced.

The phase-noise spectra of a tunable oscillator with automatic carrier suppression measured at different offsets from the SLC resonator resonant frequency are shown in Fig. 9. For instance, curve 1 gives the phase-noise spectrum at $f_{\rm osc} = f_{\rm res}$. In this case, the spectral density of the phase noise equal to -145 dBc/Hz at $f = 1$ kHz. The 5-dB noise degradation as compared with the fixed frequency oscillator (see Fig. 3) is caused by the phase noise of the VCP, which was introduced into the interferometer to enable the electric tuning of the oscillator frequency. Pulling the oscillator frequency from $f_{\rm res}$ by 5 and 10 kHz results in the phase-noise spectra given by curves 2 and 3, respectively. In the latter case, the oscillator phase noise at $f = 1$ kHz increases to the level -131 dBc/Hz. This increase is caused by amplitude fluctuations inside the interferometer and can be minimized by broadening the bandwidth of the amplitude-control system. By doing so, the oscillator phase noise at a Fourier frequency of 1 kHz should be reduced to the level of -140 dBc/Hz, which is set by oscillator AM fluctuations.

V. Conclusion

We have demonstrated potential and practical applications of the microwave interferometric technique for oscillator precision noise measurements and frequency stabilization. By using the interferometric signal processing, the phase noise of a 9-GHz oscillator operating entirely at room temperature was reduced to the level of -150 dBc/Hz at Fourier frequency $f = 1$ kHz, which was 25 dB better than state-of-the-art. The phase-noise performance of such an oscillator improves proportionally with power incident on the resonator, and a phase-noise spectral density of order $\mathcal{L}_{\varphi}^{\rm osc}(1\ {\rm kHz}) = -160$ dBc/Hz can be expected for room-temperature oscillators operating with an incident power of $P_{\rm inc} = 500$ mW.

We have also developed a tunable low phase-noise microwave oscillator with automatic carrier suppression. Such an oscillator enables a fast frequency tuning to be combined with a low phase-noise performance. It also exhibits an improved immunity to environmental disturbances such as vibrations, which normally tend to upset balance of the microwave interferometer and degrade the oscillator frequency stability. The phase-noise spectral density of a 9-GHz tunable oscillator operating at room temperature was measured to be -145 dBc/Hz at 1-kHz Fourier frequency. We expect that X-band liquid-nitrogen-cooled oscillators with automatic carrier suppression should be capable of achieving the phase-noise levels of order $S_{\varphi}^{\rm inc}(1\ {\rm kHz}) \approx -180$ dBc/Hz. Such oscillators are supposed to play a crucial role in the precision physical experiments aimed at the detection of gravitational waves.

Acknowledgment

The authors are grateful to A/Prof. D. G. Blair and Dr. A. G. Mann for their general assistance and useful discussions, and J. H. Searls, Managing Director of Poseidon Scientific Instruments Pty. Ltd., for supplying microwave and electronic equipment for noise measurements.

References

[1] W. P. N. Court, "A tunable filter for use in the measurement of excess noise from local oscillators," *Electron. Eng.*, p. 208, 1958.
[2] J. Ondira, "A microwave system for measurements of AM and FM noise specta," *IEEE Trans. Microwave Theory Tech.*, vol. MTT-16, pp. 767–781, Sept. 1968.
[3] D. G. Santiago and G. J. Dick, "Microwave frequency discriminator with a cooled sapphire resonator for ultra-low phase noise," in *Proc. IEEE Freq. Control Symp.*, Hershey, PA, June 1992, pp. 176–182.
[4] ——, "Closed loop tests of the NASA sapphire phase stabilizer," in *Proc. IEEE Freq. Control Symp.*, Salt Lake City, UT, June 1993, pp. 774–778.
[5] E. N. Ivanov, M. E. Tobar, R. A. Woode, and J. H. Searls, "Advanced phase noise suppression technique for next generation of ultra low-noise microwave oscillators," in *Proc. IEEE Freq. Control Symp.*, San Francisco, CA, June 1995, pp. 314–320.
[6] E. N. Ivanov, M. E. Tobar, and R. A. Woode, "Ultra-low noise microwave oscillator with advanced phase noise suppression system," *IEEE Trans Microwave Guided Lett.*, vol. 6, pp. 312–315, Sept. 1996.
[7] ——, "Experimental study of noise phenomena in microwave components," in *Proc. IEEE Freq. Control Symp.*, Honolulu, HI, June 1996, pp. 858–865.
[8] ——, "A study of noise phenomena in microwave components using an advanced noise measurement system," *IEEE Trans. Ultrason., Ferroelect., Freq. Contr.*, vol. 44, pp. 161–164, Jan. 1997.
[9] ——, "Microwave interferometry: Application to precision measurements and noise reduction techniques," *IEEE Trans. Ultrason., Ferroelect., Freq. Contr.*, to be published.
[10] M. M. Driscoll and R. W. Weinert, "Spectral performance of sapphire dielectric resonator-controlled oscillators operating in the 80 K to 275 K temperature range," in *Proc. IEEE Freq. Control Symp.*, San Francisco, CA, June 1995, pp. 401–412.
[11] C. A. Flory and R. C. Taber, "Microwave oscillators incorporating cryogenic sapphire dielectric resonators," in *Proc. IEEE Freq. Control Symp.*, Salt Lake City, UT, June 1993, pp. 763–773.
[12] T. E. Parker, "Characteristics and sources of phase noise in stable oscillators," in *Proc. 41st IEEE Freq. Control Symp.*, 1987.
[13] F. G. Ascarrunz, E. S. Ferre, and F. L. Walls, "Investigation of AM and PM Noise in X-band devices," in *Proc. IEEE Freq. Control Symp.*, Salt Lake City, UT, 1993, pp. 303–311.
[14] D. P. Tsarapkin and V. S. Komarov, "Microwave oscillator with combined frequency stabilization system," in *Proc. Moscow Power Eng. Inst. Theory Oscillations Radio-Transmitting Devices*, vol. 151, Moscow, Russia, 1973, pp. 82–86.

[15] S. Chang, A. G. Mann, A. N. Luiten, and D. G. Blair, "Measurements of radiation pressure effect in cryogenic sapphire dielectric resonators," *Phys. Rev. Lett.*, vol. 79. no. 11, pp. 2141–2144, Sept. 1997.
[16] R. A. Woode, M. E. Tobar, E. N. Ivanov, and D. G. Blair, "Ultra-low noise microwave oscillator based on liquid nitrogen cooled sapphire resonator," *IEEE Trans. Ultrason., Ferroelect., Freq. Contr.*, vol. 43, pp. 1936–1941, May 1996.
[17] A. N. Luiten, A. G. Mann, and D. G. Blair, "Improved sapphire dielectric resonators for ultrastable oscillators," in *Proc. IEEE Freq. Control Symp.*, Salt Lake City, UT, June 1993, pp. 757–761.
[18] A. A. Andronov, A. A. Vitt, and S. E. Khaikin, *Theory of Oscillators* (Int. Series of Monographs in Physics 4). New York: Pergamon, 1966, ch. 8, pp. 583–613.

Eugene N. Ivanov was born in Moscow, Russia, on August 14, 1956. He received the Ph.D. degree in radio electronics from the Moscow Power Engineering Institute, Moscow, Russia, in 1987.

From 1980 to 1990, he was involved in the design of low-noise Gunn diode oscillators and analysis of electromagnetic dielectric resonators with whispering gallery modes. In 1991, he joined the Gravitational Research Laboratory, University of Western Australia, Nedlands, W.A. In 1993, he developed a microwave readout system for the cryogenic resonant-mass gravitational wave detector "Niobe." In 1995, he suggested a new frequency-stabilization technique, which resulted in 25-dB improvement in the phase-noise performance of X-band oscillators. In 1996, he designed a microwave interferometric noise-measurement system with sensitivity approaching the thermal noise limit. The extremely low-noise floor of such a system close to -193 dBc/Hz at 1-kHz Fourier frequency allowed the first experimental evidence of intrinsic $1/f$ noise in microwave isolators.

Dr. Ivanov is a corecipient of the 1994 Japan Microwave Prize.

Michael E. Tobar (S'87–M'88–A'90) was born in Maffra, Australia, on January 3, 1964. He received the B.Sc. degree in theoretical physics and mathematics and the B.E. degree with honors in electrical and computer systems engineering from Monash University, Melbourne, Australia, in 1985 and 1988, respectively.

From 1989 to 1992 he was with the Department of Physics, University of Western Australia, Nedlands, W.A., where he was appointed a Research Associate from 1992 to 1993. He is currently an Associate Post-Doctoral Research Fellow at the University of Western Australia. His research interests include low-noise oscillators, measurement systems and components, ultrasensitive transducers, quantum measurement, gravitational wave detection, cryogenic systems, electromagnetics, microwaves, optics, and mathematical modeling.

Richard A. Woode was born in Bishops Stortford, U.K., on January 2, 1966. He received the honors degree in mechanical engineering from the University of Portsmouth, Portsmouth, U.K., in 1989, and the Ph.D. degree from the University of Western Australia, Nedlands, W.A., in 1998.

In 1989, he joined the research team of Edwards High Vacuum International, Crawley, U.K., where he worked as a Research and Development Engineer for over three years, leaving in 1993 to continue with his interest in physics. He is also interested in the research areas of high-stability microwave oscillators, mechanical systems, optics, and control.